Fuel 217 (2018) 262–274

Contents lists available at ScienceDirect

Fuel

journal homepage: www.elsevier.com/locate/fuel

Full Length Article

Analytical solution for steam-assisted gravity drainage with consideration of temperature variation along the edge of a steam chamber

Xiaoxing Shi[a], Ryosuke Okuno[b,*]

[a] University of Alberta, Canada
[b] University of Texas at Austin, USA

ARTICLE INFO

Keywords:
Steam-assisted gravity drainage
Bitumen
Analytical model
Steam-chamber-edge temperature
Steam-oil ratio

ABSTRACT

Steam-assisted gravity drainage (SAGD) is a widely-used method for heavy-oil and bitumen recovery. Analytical SAGD models presented in the literature often overestimate bitumen-production rate substantially. Although bitumen-production rate and steam-oil ratio (SOR) depend significantly on temperature near the steam-chamber edge in SAGD, previous analytical models assumed the injected-steam temperature to uniformly distribute along the edge of a steam chamber. The main objective of this research is to develop the first analytical SAGD model that takes into account temperature variation along the edge of a steam chamber.

Local material balance and Darcy's law are applied to each cross section perpendicular to the edge of a steam chamber. Then, they are coupled with the global material balance for the chamber geometry that is an inverted triangle. New analytical equations are presented for bitumen-production rate and SOR, in addition to associated variables as functions of elevation from the production well, such as oil-flow rate and temperature along a linear chamber edge. Bitumen-production rate and SOR can be calculated for a representative chamber-edge temperature at a certain elevation from the production well.

Comparison of the analytical model with numerical simulations shows that bitumen-production rate and SOR can be accurately estimated when the new model is used with the temperature taken from the midpoint of the edge of a steam chamber. The chamber-edge temperature used for the new analytical model that gives accurate results can be up to 100 Kelvin lower than the injected steam temperature for a given operating pressure in the cases tested. The previous assumption of the injected-steam temperature at the chamber edge gives overestimated oil-production rates for SAGD. The constant temperature along the edge of a steam chamber gives Butler's concave interface of a steam chamber that is detached from the production well. For a chamber to exhibit a linear interface, temperature must vary along the chamber edge, which occurs in reality mainly because of heat losses to the over- and under-burden formations.

1. Introduction

Steam-assisted gravity drainage (SAGD) is a widely-used method for in-situ recovery of bitumen. In SAGD, high-quality steam (e.g., 90%) is injected into a bitumen reservoir through a horizontal well. The injected steam forms a steam chamber, and condenses near the edge of a steam chamber, where latent heat is released upon steam condensation. Along the edge of a steam chamber, the heated, mobile bitumen and hot water flow toward another horizontal well, which is located approximately 5 m below and parallel to the injection well.

Bitumen is extremely viscous, and usually not mobile at original reservoir conditions. However, bitumen viscosity is highly sensitive to temperature; e.g., it can decrease from several million centipoise (cp) at original reservoir temperatures to below 10 cp at 400 K [1]. This sensitivity of bitumen viscosity to temperature makes SAGD applicable for in-situ bitumen recovery. Recently, coinjection of steam and solvent has been also studied to improve thermal efficiency of SAGD [2–4]. In such coinjection processes, operating steam-chamber temperatures are lower than those in SAGD, because vapor-condensation temperature becomes lower in the presence of volatile solvents at a given operating pressure. This tends to reduce the amount of heat conduction to the overlaying formation rocks during bitumen recovery. Hence, chamber temperature plays an important role in in-situ bitumen recovery in terms of oil-production and energy efficiency.

Many analytical studies have been conducted to understand primary factors affecting bitumen production, and to estimate bitumen-recovery

* Corresponding author at: Hildebrand Department of Petroleum and Geosystems Engineering, University of Texas at Austin, 200 E. Dean Keeton Street, Stop C0300, Austin, TX 78712, USA.
E-mail address: okuno@utexas.edu (R. Okuno).

https://doi.org/10.1016/j.fuel.2017.12.110
Received 10 March 2017; Received in revised form 3 December 2017; Accepted 22 December 2017
Available online 02 January 2018
0016-2361/

Nomenclature

SAGD steam-assisted gravity drainage
SOR steam-oil ratio

Greek Symbols

α thermal diffusivity of reservoir
β_θ parameter used to describe the extent to which flow direction deviates from steam chamber edge
θ angle between steam chamber edge and horizontal
θ_{ave} average angle of oleic flow along the chamber edge
μ dynamic viscosity
ν kinematic viscosity
ξ distance normal to the steam chamber edge
ρ density
τ term defined by Eq. (A.8)
φ porosity of reservoir
ω acentric factor

Roman Symbols

a an empirical constant used in Reis' model
a_1, a_2, a_3, a_4 density correlation constants in Eq. (12)
g gravitational acceleration
H vertical distance from reservoir top to the production well
h_i equals to one-meter in this paper
I_o integration of kinematic viscosity of oil phase in the cross-section perpendicular to steam chamber edge
k permeability
k_{rave} average value of relative permeability in each cross-section ahead of steam chamber
l distance starting from production well in the direction along steam chamber edge
M volumetric heat capacity
N_L number of one-meter layers used in the calculation of SOR with Eq. (9)
q_o oil flow rate
$q_{oil\text{-}prod}$ oil production rate at the production well
ΔS_o reducible oil saturation of reservoir
T temperature
U chamber edge advancing velocity that is normal to the edge
U_o flow velocity of oleic phase along steam chamber edge
v chamber edge advancing velocity in horizontal direction
v_{max} chamber edge advancing velocity at the reservoir top
W_s width of steam chamber at reservoir top
x mole fraction of a component in the L phase
Δy unit length in the direction along the production well
z elevation

Subscript

ceiling contact area between steam chamber and overburden layer
D dimensionless
e steam chamber edge
L the point where the perpendicular line from steam chamber edge ξ intersects with production layer
R under reservoir condition
s at steam temperature
o oleic phase
over overburden formation properties

efficiency in SAGD. Butler et al. [5] presented the first analytical SAGD model by combining material balance and Darcy's law as

$$q_{oil\text{-}prod} = 2\Delta y\sqrt{2kg\alpha\varphi\Delta S_o H/(m\nu_s)},$$

where $q_{oil\text{-}prod}$ is the oil production rate; Δy, k, g, α, φ, ΔS_o, H, and ν_s are the unit length of the horizontal production well, permeability, gravity constant, thermal diffusivity, difference between initial oil saturation and residual oil saturation, reservoir thickness and oil kinematic viscosity at the steam temperature, respectively. m is a constant reflecting the sensitivity of kinematic viscosity to temperature, and is defined in $\nu_s/\nu_o = [(T-T_R)/(T_S-T_R)]^m$ [6], where ν_o, T_S, and T_R are oil kinematic viscosity, steam temperature and initial reservoir temperature, respectively. The value of m is considered to be 3–4 for bitumen and heavy oil. Butler et al. [5] assumed the chamber-edge temperature (T_e) to be the steam temperature (T_S) at the operating pressure. Furthermore, T_e was assumed to uniformly distribute along the interface of a steam chamber. This assumption yields a concave edge of a steam chamber that extends to infinity at the reservoir top, and is detached from the production well.

Butler and Stephens [6] presented the "Tandrain" model by changing the constant 2.0 to 1.5 inside the square root in the equation given above, assuming that the bottom of a steam chamber was fixed at the production well. Later, Butler [7] proposed another model called "Lindrain" by changing the constant to 1.3, assuming a straight steam-chamber edge tangent to the production well. Calculation results from these revised models were more accurate than the equation given above. However, they still overestimated bitumen-production rates in SAGD.

Reis [8] proposed another SAGD model with a linear steam-chamber edge, which has been widely used:

$$q_{oil\text{-}prod} = 2\Delta y\sqrt{kg\alpha\varphi\Delta S_o H/(2am\nu_s)},$$

where the constant "a" was empirically set to 0.4, which is equivalent to replacing the constant 2.0 by 0.8 inside the square root in the equation of Butler et al. [5]. With the assumed chamber geometry of an inverted triangle, Reis applied material balance globally to the entire mobile-bitumen zone. Although Reis' equation gives a lower bitumen-production rate than the equation of Butler et al. [5], Tandrain, and Lindrain, it still tends to overestimate SAGD's bitumen production.

Various prior models added different considerations by making various modifications to the models of Butler et al. [5] and Reis [8]. Some modified the fluid model in Butler et al.'s models [5–7]. Bharatha et al. [9] considered the effect of dissolved gas on bitumen viscosity. Sharma and Gates [10] took into account a relative-permeability distribution ahead of the edge of a steam chamber. Mojarad and Dehghanpour [11] considered emulsion flow ahead of the edge of a steam chamber. Some studies modified Butler et al.'s model [5] in terms of reservoir properties. Cokar et al. [12] considered the effect of volumetric heat expansion on production in their analytical model. Irani and Cokar [13] considered the dependence of reservoir properties on temperature, and used local reservoir properties in their calculation. Studies based on Reis' model [8] include Akin [14], who considered the effect of asphaltene deposition on the oil-phase viscosity, and Azad and Chalaturnyk [15], who considered permeability heterogeneity in their analytical model.

All prior studies assumed that the chamber-edge temperature is equal to the injected-steam temperature at an operating pressure. However, observations from simulation results and field data [16,17] indicate that T_e varies along the edge of a steam chamber. Then, the main objective of this research is to develop the first analytical SAGD model that accounts for a temperature variation along a linear steam-

chamber edge. Unlike prior SAGD models, the resulting model requires a representative chamber-edge temperature as one of the input parameters for analytical solution of SAGD, as will be shown in this paper. This paper also discusses a few major simplifying assumptions used in the analytical model, i.e. 1-D single-phase flow along the chamber edge and 1-D heat conduction.

The central question that initially motivated this research was how temperature is supposed to change along the edge of a steam chamber for a given bitumen production rate. As will be shown in this paper, the conventional assumption of constant chamber-edge temperature is not necessary to derive an analytical equation for bitumen-production rate for SAGD. This research analytically clarifies that assumption of a certain chamber geometry implicitly results in a certain temperature distribution along the edge of a steam chamber. This clarification is the most fundamental novelty of this paper. This research also clarifies that Butler's chamber geometry is caused by the assumption of a constant temperature (i.e., the wet-steam temperature at the operating pressure) along the chamber edge. The general framework presented for the derivation in this paper is expected to yield a different analytical model for a different chamber geometry (e.g., a simple polynomial function to represent a certain chamber-growth pattern), although such an extension is beyond the scope of the current paper.

2. Theory

This section presents a concise derivation of bitumen-production rate and steam-oil ratio for SAGD in the side-way expansion stage after a steam chamber has reached the reservoir top. The derivation consists of three main components: local material balance applied to a cross section perpendicular to the edge of a steam chamber, Darcy's law applied to oil flow along the edge of a steam chamber, and global material balance. The derivation is general in that it yields a unified framework for the models of Butler et al. and Reis, their variants, and this research by use of their corresponding assumptions [18].

The assumptions made in this paper, which are commonly used in the literature [7–9], are as follows:

1) A steam chamber is an inverted triangle with its vertex fixed at the production well.
2) Laminar flow parallel to the edge of a steam chamber
3) Homogeneous, isotropic reservoir
4) No chemical reaction
5) No interaction between fluid and rock
6) Incompressible oil
7) Negligible capillary pressure
8) Vapor-phase flow parallel to the edge of a steam chamber is negligible
9) Density of vapor phase is negligible in comparison with that of oil phase
10) Constant permeability to the oil phase ahead of the edge of a steam chamber
11) 1-D quasi-steady state heat conduction through the moving interface of a steam chamber
12) Heat losses to under and overlaying formation rocks.

Fig. 1 shows a schematic for the derivation, which only accounts for one half of the reservoir. Assumption 12 is part of Assumption 1; that is, a linear edge of a steam chamber is unlikely without heat losses to under and overlaying formation rocks [18]. Assumption 11 indicates that heat transfer is calculated only based on a temperature gradient in the direction of interest; e.g., the perpendicular direction to the edge of a steam chamber, and the perpendicular direction to the reservoir top and bottom lines. This is not called 2-D heat transfer because a temperature gradient parallel to the interface is assumed not to affect the heat transfer.

In Appendix A1, the local material balance and Darcy's law are coupled to derive the derivative of oil flow rate, q_o, with respect to elevation z as follows:

$$\frac{\partial q_o^2}{\partial z} = -2\varphi \Delta S_o k g \tau (\Delta y)^2 \tag{1}$$

for the cross-section perpendicular to the edge of a steam chamber at elevation z. As shown in Appendix A2, this equation can be used also for Butler et al.'s model and its variants. In the above equation, τ is the dimensionless variable defined in Eq. (A.8).

Eq. (1) is applied to the assumed linear edge of a steam chamber. Then, the chamber-edge advancing velocity in the horizontal direction varies linearly with elevation z as follows:

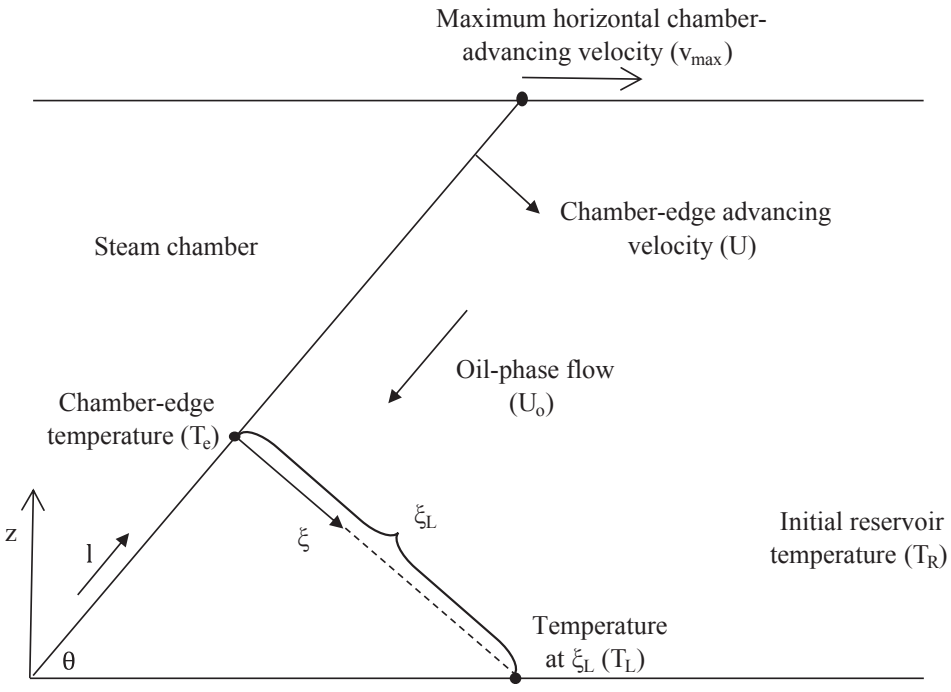

Fig. 1. Schematic for oil flow along the edge of a steam chamber in SAGD for the developed analytical model.

$$v = z v_{max}/\ H = v_{max} z_D, \tag{2}$$

where v_{max} is the maximum chamber-advancing velocity in the horizontal direction at the reservoir top; H is the vertical distance between the reservoir top and the production well; and dimensionless elevation z_D is defined as $z_D = z/H$. Combining Eq. (1) with Eq. (2) gives the following:

$$\frac{\partial q_o}{\partial z} = \varphi \Delta S_o v_{max} z_D \Delta y \tag{3}$$

for the cross-section at elevation z. Integration of Eq. (3) gives

$$q_o(z) = \varphi \Delta S_o v_{max} \Delta y z^2/(2H) + C, \tag{4}$$

where C is the constant of integration.

Finally, C is evaluated by use of the global material balance of Reis [8] for a half of an inverted-triangle chamber. That is,

$$q_o|_{z=0} = C = -\varphi \Delta S_o H v_{max} \Delta y/2 = -q_{oil\text{-}prod}, \tag{5}$$

where $q_{oil\text{-}prod}$ is the rate of oil production at the production well located at z = 0. The negative sign for $q_{oil\text{-}prod}$ arises due to the notation used for Darcy's law that q_o is positive in the upward direction along the edge of a steam chamber (the l direction in Fig. 1). Substituting Eq. (5) into Eq. (4),

$$q_o(z_D) = -\varphi \Delta S_o H \Delta y v_{max}(1-z_D^2)/2 = (1-z_D^2) q_o|_{z=0}. \tag{6}$$

Eq. (6) dictates the profile of q_o along the edge of a linear chamber edge. Using Eqs. (2), (5) and (A.9),

$$v_{max} = (k g \tau \Delta y)/[z_D(1-z_D^2) q_{oil\text{-}prod}]. \tag{7}$$

Substitution of Eq. (7) into Eq. (5) yields

$$q_{oil\text{-}prod} = \sqrt{\tau k g H \varphi \Delta S_o (\Delta y)^2/[2(1-z_D^2) z_D]}, \tag{8}$$

where the negative solution for $q_{oil\text{-}prod}$ was discarded, and τ was defined as a function of elevation (z or z_D) by Eq. (A.8). Eq. (8) is obviously independent of z_D because of the global material balance, Eq. (5), within the current derivation based on the assumptions listed previously. That is, Eq. (8) describes the consistency to be satisfied among the variables and assumptions used; in particular, the relationship between the vertical profile of chamber-edge temperature, $T_e(z_D)$, and production rate, $q_{oil\text{-}prod}$.

This analytical model of SAGD does not require an injected-steam temperature to solve for production rate. Instead, it requires a temperature from somewhere along the edge of a steam chamber as part of the input information. As will be shown later in this paper, however, a representative temperature should be taken from, or estimated for the mid-elevation range along the edge of a steam chamber for accurate estimation of oil-production rate and SOR.

Calculation of SOR can also be derived according to the aforementioned assumptions and equations (Appendix B). The final equation for SOR calculation is as follows:

$$\mathrm{SOR} = [1/(\rho_w L_s x)] \left\{ \begin{array}{l} 0.5 M_R (T_S - T_R) v_{max} H \Delta y + \sum_{i=1}^{N_L} 2 M_R [T_{e(z)} - T_{L(z)}] \alpha h_i \Delta y \\ \quad /(z \tan\theta) \\ + 2 M_{over} (T_{ceiling} - T_R) \Delta y \sqrt{\alpha v_{max} W_S/\pi} + q_{oil-prod} (T_S - T_R) M_o \end{array} \right\} / q_{oil\text{-}prod}, \tag{9}$$

where ρ_w is the mass density of water in (kg/m^3); L_S is the latent heat carried by the injected steam in J/kg; x is steam quality; M_R, M_{over} and M_o are the volumetric heat capacity of reservoir, overburden formation and bitumen in ($J \cdot m^{-3} \cdot K^{-1}$), respectively; T_S is injected-steam temperature in K; N_L is the number of one-meter layers; h_i is set to one meter in this paper; $T_{ceiling}$ is the temperature at the bottom of the overburden formation which is assumed to be T_S over the contact area; and W_S is the width of the ceiling of the half steam chamber.

A step-wise description of the algorithm that calculates oil-production rate is given below.

1. Obtain the reservoir and bitumen properties, such as reservoir thickness (H), horizontal-section length (Δy), reservoir temperature (T_R), operation pressure (P), permeability (k), mobile-oil saturation (ΔS_o), porosity (φ), thermal diffusivity (α), a relationship between temperature and bitumen kinematic viscosity, and steam-chamber-edge temperature around the midpoint along the steam-chamber edge (T_e).
2. Set T_L to T_R at the midpoint.
3. With the T_e value taken from the middle elevation, use Eq. (A.8) to calculate the value of τ for $z_D = 0.5$.
4. Substitute the resulting τ value into Eq. (8), and calculate oil-production rate, $q_{oil\text{-}prod}$.
5. Use the calculated $q_{oil\text{-}prod}$ to calculate a new T_L according to Eqs. (2) and (5), and Eq. (A.7). Use the new T_L to calculate $q_{oil\text{-}prod}$ by repeating steps 3, 4, and 5 until the new $q_{oil\text{-}prod}$ becomes close to the previous value (e.g., deviation less than 1.0 m^3/day).

With the obtained $q_{oil\text{-}prod}$, Eq. (8) can be solved for $\tau(z_D)$. Furthermore, Eq. (A.8) can be solved for T_e as a function of z, or z_D.

3. Model validation and discussion

This section firstly presents validation of the analytical solution given in Section 2 against results from reservoir flow simulations. Simulation cases used for the validation are made consistent with the assumptions used for the analytical model as much as possible, as listed in Section 2. However, some assumptions in the analytical model cannot be set explicitly as part of the input information for a simulation model. In this section, therefore, analysis is also conducted for the following assumptions made in the analytical solution: 1-D quasi-steady state heat conduction ahead of the chamber edge, and 1-D single-oil-phase flow along the edge of a steam chamber. All simulation cases in this research are performed by use of the STARS simulator of Computer Modelling Group [20].

This section will explain why T_e in the analytical solution should be taken from the midpoint along the edge of a linear steam chamber. Additionally, the difference of the new analytical model from Butler et al.'s and Reis' models in terms of T_e will be clarified, which emphasizes the importance of considering temperature variation along the chamber edge in analytical solution of SAGD.

3.1. Validation of the new analytical model

Only one half of a steam chamber is simulated in Section 3. Dimensions of the simulation model are 70.0 × 37.5 × 20.0 m^3 in the x, y, and z directions, respectively. This homogeneous reservoir is discretized into 140 × 1 × 20 grid blocks in the x, y, and z directions, respectively. The injection well is situated at the 14th layer from the top, while the production well is at the 18th layer from the top of the reservoir. Both wells are located in the left-most column of the reservoir model. Reservoir temperature and pressure are initially at 286.15 K and 15 bara. Table 1 lists pertinent reservoir properties used in the simulation cases.

The phase behavior model in the simulation cases uses three components: methane, bitumen, and water. Properties of the bitumen component were taken from Kumar and Okuno [21]. Table 2 shows the components' critical pressure, critical temperature, and acentric factor. Water dissolution in the oleic (L) phase is not considered in the main simulation case in this section; hence, K-values for hydrocarbon

Table 1
Reservoir properties used for analytical calculations and simulations in Section 3.

Property	Unit	Value
Porosity	–	0.33
Initial oil saturation	–	0.75
Initial water saturation	–	0.25
Residual oleic phase saturation	–	0.13
Residual liquid saturation	–	0.38
Oil phase relative permeability at irreducible water saturation (k_{rocw})	–	1
Relative permeability at water at residual oil saturation (k_{rwro})	–	0.3
Gas phase relative permeability at connate liquid saturation (k_{rg})	–	0.3
Exponent for Corey's relative permeability for all phases	–	1
Initial reservoir temperature (T_R)	K	286.15
Temperature of injected steam (T_S)	K	515.71
Initial reservoir pressure	bara	15
Steam quality	–	0.9
Latent heat of injected steam (L_S)	J/kg	1.75×10^6
Maximum bottom-hole pressure for injector	bara	35
Minimum bottom-hole pressure for producer	bara	15
Horizontal well length (Δy)	m	37.5
Maximum surface liquid rate for producer	m^3/day	200
Maximum steam rate for producer	m^3/day	1
Permeability (k)	mD	4000
Rock heat capacity	kJ/(m^3·K)	2600
Rock thermal conductivity	J/(m·day·K)	6.60×10^5
Bitumen thermal conductivity	J/(m·day·K)	1.15×10^4
Gas thermal conductivity	J/(m·day·K)	2892
Water thermal conductivity	J/(m·day·K)	1.50×10^5

Table 2
Components' properties used for the equation-of-state model [21]

Component	MW, g/mol	Tc, K	Pc, bara	ω
Methane	16.04	190.60	46.00	0.0080
Bitumen	530.00	847.17	10.64	1.0406
Water	18.01	647.10	220.64	0.3433

components are represented by the Peng-Robinson equation of state (PR EOS) [22] and those for water are represented by Raoult's law.

L-phase viscosity in the STARS simulator is calculated by the following mixing rule:

$$\mu_o = \exp\left(\sum x_i \ln \mu_i\right), \tag{10}$$

where i = {methane, bitumen, water}, μ_o is L-phase viscosity, x_i is mole fraction of component i in the L phase, and μ_i is dynamic viscosity of component i. Table 3 shows components' viscosities at different temperatures under the operation pressure, 35 bara [23].

L-phase molar density in the STARS simulator is calculated by the following mixing rule (no volume change on mixing):

$$1/\rho_o = \sum (x_i/\rho_i), \tag{11}$$

where i = {methane, bitumen, water}, ρ_o is L-phase molar density and ρ_i is the molar density of component i. The analytical model assumes the L phase to be incompressible. To make the simulation model consistent with the analytical model, bitumen is set to be incompressible. However, methane, a compressible gas, is present in the L phase in the simulation model. Molar densities of methane and water (mol/m^3) are represented in terms of pressure (P) and temperature (T) as follows:

$$\rho_i = \rho_{ii}\exp[a_1(P-1.01325) - a_2(T-288.15) - 0.5a_3(T^2-288.15^2) + a_4(P-1.01325)(T-288.15)], \tag{12}$$

where ρ_{ii} is the molar density of component i under reference condition. $\rho_{ii} = 2.00 \times 10^4$ mol/m^3, $a_1 = 5.13 \times 10^{-6}$ $bara^{-1}$, $a_2 = 1.32 \times 10^{-3}$ K^{-1}, $a_3 = 5.77 \times 10^{-6}$ K^{-2}, and $a_4 = 4.05 \times 10^{-8}$ $K^{-1}bara^{-1}$ for methane; $\rho_{ii} = 5.54 \times 10^4$ mol/m^3, $a_1 = 0.00$ $bara^{-1}$, $a_2 = -1.67 \times 10^{-3}$ K^{-1}, $a_3 = 6.48 \times 10^{-6}$ K^{-2}, and $a_4 = 0.00$ $K^{-1}bara^{-1}$ for water.

Based on Eqs. (11) and (12), L-phase density at 35 bara is calculated to be 992.64 kg/m^3 at the steam saturation temperature, while it is 977.69 kg/m^3 at the initial reservoir temperature. Hence, the change in L-phase density caused by compressible methane is only 1.5%, which is deemed negligible.

As mentioned previously, some assumptions made in the analytical model cannot be set explicitly in the simulation model. At early times in the simulation, a chamber edge is still developing to be linear, even in the side-way expansion stage (assumption 1). At later times, however, water condensate accumulates at higher levels near the edge of a steam chamber, which deviates from the assumption of single-oil-phase flow (assumption 10). Fig. 2 shows that the accumulation of water ahead of the edge of a steam chamber increases with decreasing chamber-edge angle, or with increasing bitumen production, in the current simulation case. Accumulation of water condensate near the edge of a steam chamber also makes the simulation model deviate from the assumption of 1-D heat conduction (assumption 11) because multi-dimensional convective flow of hot water causes heat convection.

Therefore, an appropriate time for validation of the analytical model against the simulation model is when the edge of a steam chamber becomes linear. This status in the simulation model is referred to as Status I in this paper. Comparison between the analytical and simulation models is also conducted at a later time, to highlight the deviation of the simulation model from the analytical model. This status in the simulation model at a later time is referred to as Status II in this paper.

In the current simulation case, Status I is reached at 75 days of injection/production operation, when the angle of the steam chamber edge, θ, is 43° (11% oil recovery). Status II is selected when θ is 28° (18% oil recovery). The value for T_e is taken from the midpoint of the chamber edge, as mentioned in Section 2, which is 487.7 K under Status I and 488.7 K under Status II.

Following the procedure described in Section 2, calculation results at Status I are obtained as given in Table 4. The analytical model yields 12.8 m^3/day, which is close to the simulated value, 12.9 m^3/day, for bitumen production rate. Other analytical models overestimate the bitumen production rate as shown in Table 4. Reis's model and the Lindrain model give similar values of bitumen production rate for this case at Status I, and they are more accurate than Butler's model and the Tandrain model.

All analytical models compared here are based on the widely-used set of assumptions for analytical solution of SAGD, including single-oil-phase flow ahead of the chamber edge. This assumption is less accurate at later times because of increasing accumulation of water condensate, as explained with Fig. 2. Fig. 3 compares the bitumen production rates

Table 3
Components' viscosity at 35 bara [23]

Temperature, K	Oil viscosity, cp	Methane viscosity, cp	Water viscosity, cp
283.15	2457801.75	38.54	1.3117
303.15	114116.11	22.59	0.798
323.15	10642.80	14.15	0.5453
343.15	1650.00	9.36	0.4028
363.15	422.00	6.48	0.3144
383.15	133.00	4.66	0.2555
403.15	58.70	3.46	0.2141
423.15	31.00	2.65	0.1835
443.15	18.30	2.07	0.1603
463.15	12.50	1.66	0.1421
483.15	9.24	1.35	0.1275
503.15	7.31	1.12	0.1155
523.15	6.10	0.94	0.1055

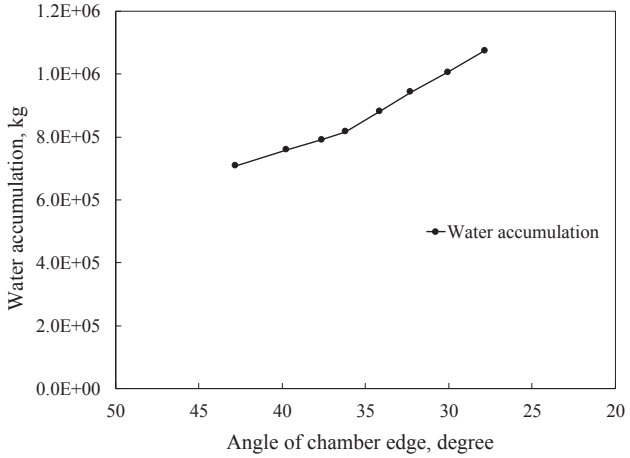

Fig. 2. Accumulation of water ahead of the edge of a steam chamber increases with decreasing chamber-edge angle, or with increasing bitumen production, in the simulation case (Table 1).

Table 4
Comparison of analytical models and simulation results in terms of bitumen-production rate under State I.

	Production rate, m^3/day	Absolute deviation	Relative deviation
Simulation	12.8751	–	–
This research	12.8219	−0.0532	−0.0041
Butler et al. [5]	19.0218	6.1466	0.4774
Tandrain [6]	16.4733	3.5982	0.2795
Lindrain [7]	15.3358	2.4607	0.1911
Reis [8]	15.0380	2.1629	0.1680

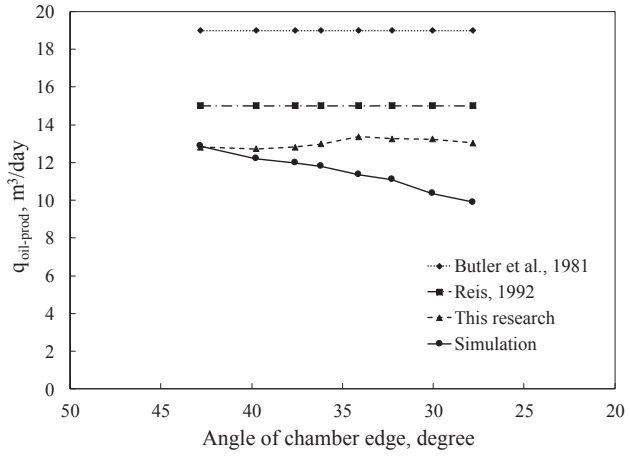

Fig. 3. Comparison of the bitumen production rates from the simulation, the new model, Butler et al.'s, and Reis' at different chamber angles.

from the simulation, the new model, Butler et al.'s, and Reis' at different chamber angles. The simulated production rate decreases as production proceeds because of increasing impact of multi-dimensional two-phase flow on bitumen-production rate as discussed in Section 3.2. Table 5 shows details of the comparison at Status II. Although the new model overestimates the bitumen production rate at Status II, it is systematically more accurate than Butler et al.'s and Reis' as shown in Fig. 3. These results also illustrate that the developed model is most accurate at conditions close to Status I.

The simulation gives an instantaneous SOR of 4.10 at Status I, which is reasonably represented by analytical models. The developed model gives 3.83, and Reis' SOR model gives 3.54 at Status I. The temperature at the boundary between the steam chamber and overlaying formation in the analytical SOR calculations is set to the steam temperature, T_S, according to the simulation.

The main difference of the new analytical model from other models in the literature is that τ is not assumed to be constant in the new model. The relationship between τ and elevation (or dimensionless elevation z_D) was analytically derived from the requirement of a linear chamber edge for a given bitumen production rate in the new model (Section 2). Fig. 4 shows the τ profiles for the new model, Butler et al.'s, and Reis' model on the basis of the current case (Table 1). The constant τ for Butler et al.'s model yields a concave edge of a steam chamber, which is unlikely under heat losses to the overlaying formation rocks, and the detachment of the chamber edge from the producing well. Reis' τ, which is also constant, is 2.5 times greater than Butler et al.'s value. Reis' constant τ is inconsistent with his assumption of linear chamber edge, which is caused by the inconsistent use of global material balance in his derivation as mentioned in Appendix A (Eq. (A.14)). Fig. 5 shows the resulting profiles of L-phase flow rate from the new model and Butler et al.'s. These two models assume different geometries of a steam chamber, and this figure clearly shows that the assumed chamber geometry dictates the profile of L-phase flow rate. Reis' profile for L-phase flow rate cannot be obtained since Reis' model only gives bitumen production rate, which is the absolute value of L-phase flow rate at $z = 0$ (Eq. (A.15)).

This section showed that assumption of a certain chamber geometry implicitly gives a certain temperature (or τ) distribution along the edge of a steam chamber. Note that the analytical model for oil-production rate in SAGD does not require details of heat losses to the over and underburden. The linear edge of a steam chamber used for the global material balance is considered as a consequence of complex energy balance, including heat losses to the over and underburden.

Although not shown in this paper, the analytical model has been validated for various simulation cases, as presented in [18], for different permeabilities, methane concentrations in the original oil, water solubilities in oil, and water compressibilities. Since water solubilities in oil can be quite high in SAGD [24–27], key results for the water-dissolution case are briefly discussed here. The phase-behavior model in this case uses the PR EOS for all three components, methane, bitumen, and water, along with optimized binary interaction parameters as given in Venkatramani and Okuno [23]. The simulation reaches Status I after 78 days of injection/production operation when the angle of the chamber edge becomes 35° (16% oil recovery). The simulation model gives 15.7 m^3/day of bitumen production rate at Status I, which is higher than the no-water-dissolution case discussed previously (Table 4). The new analytical model gives 15.8 m^3/day, which is nearly identical with the simulated value. Other models substantially overestimate the bitumen production rate; Bulter et al.'s, the Tandrain model, the Lindrain model, and Reis' model respectively give 28.9 m^3/day, 25.0 m^3/day, 23.3 m^3/day, and 22.8 m^3/day. It was observed that the advantage of the new model over other models is more significant when bitumen-production rate is higher; e.g., for cases with higher absolute permeabilities [18].

Table 5
Comparison of analytical models and simulation results in terms of bitumen-production rate under State II.

	Production rate, m^3/day	Absolute deviation	Relative deviation
Simulation	9.8986	–	–
This research	12.9863	3.0877	0.3119
Butler et al. [5]	19.0218	9.1232	0.9217
Tandrain [6]	16.4733	6.5747	0.6642
Lindrain [7]	15.3358	5.4372	0.5493
Reis [8]	15.0380	5.1394	0.5192

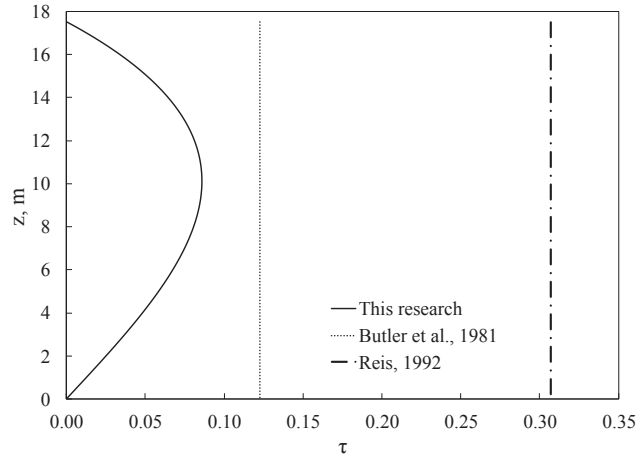

Fig. 4. Profiles of τ for the new model, Butler et al.'s, and Reis' model on the basis of the case given in Table 1.

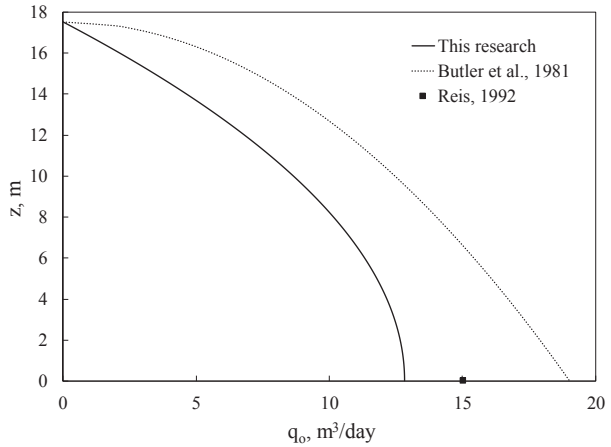

Fig. 5. Profiles of L-phase flow rate from the new model and Butler's. This figure clearly shows that the assumed chamber geometry dictates the profile of L-phase flow rate. Reis' profile for L-phase flow rate cannot be obtained since Reis' model only gives the L-phase flow rate at z = 0.

3.2. Discussion

The analytical calculation uses the T_e value taken from the midpoint of the linear edge of a steam chamber. This selection of T_e was primarily informed by many comparisons of T_e profiles along the chamber edge from the analytical and numerical simulation models in this research. In this section, temperature distribution ahead of a steam chamber is discussed in the context of the interplay between phase flow and heat transport in SAGD. This will explain why T_e from the midpoint is chosen for the current analytical solution.

3.2.1. Temperature distribution ahead of a steam chamber

Fig. 6 shows that the analytical T_e profile is close to the simulated values in the elevation range of 7–16 m at Status I (no-water-dissolution case). The underestimated T_e values at lower elevations come from various simplifying assumptions, most directly from the 2-D two-phase flow and 2-D heat transfer in simulation. In the analytical solution, the τ profile is obtained for a specified bitumen production rate under the set of assumptions, such as single-phase flow of oil. The analytical τ so calculated tends to underestimate the chamber-edge temperature where the oil-phase mobility is overestimated by not considering oil/water two-phase flow. More details are explained below.

Fig. 7 depicts the simulated and analytically-calculated profiles of temperature perpendicular to the chamber edge at z of 3 m (Fig. 7a) and 9 m (Fig. 7b). The difference between two plots at the chamber edge (0 m) corresponds to the difference shown in Fig. 6 at the corresponding z values. At z of 3 m near the reservoir bottom, the temperature difference is approximately 50 K at the chamber edge. As a result, the temperature profiles beyond the chamber edge are also different from each other. At z of 9 m near the midpoint of the chamber edge, the analytical and simulated profiles of temperature are close to each other.

The deviations observed near the bottom and top of the reservoir model come from coupled effects of several simplifying assumptions in the analytical model, such as 1-D quasi-steady-state heat conduction from a moving interface, and 1-D single-oil-phase flow parallel to the chamber edge. In terms of the former assumption, Butler [28] and Keshavarz et al. [29] discussed that this assumption is not accurate near the top and bottom of the reservoir for SAGD analytical solution. The advancing velocity of a linear chamber edge monotonically decreases with decreasing elevation until it becomes stationary at the production well (see Fig. 1). Hence, the effect of a moving boundary on heat conduction beyond the chamber edge diminishes near the bottom of the reservoir. Near the top of the reservoir, on the other hand, the presence of the overlaying formation makes the assumption of 1-D heat conduction inaccurate since multi-dimensional heat conduction inevitably occurs there. The applicability of one-dimensional steady-state heat conduction from a moving boundary to SAGD problems were also discussed in [8,9]. In the subsequent subsections, this issue is revisited from the view point of two-phase flow ahead of a steam chamber.

3.2.2. Multi-Dimensional flow ahead of a steam chamber

L-phase flow ahead of a steam chamber is assumed parallel to the chamber edge in all analytical SAGD models, including the current one. Fig. 8 shows the distribution of L-phase flow vectors in the simulation at Status I. Arrows in the figure represent L-phase flow directions and their magnitudes. It clearly shows that L-phase flow near the bottom of the reservoir is far from being parallel to the chamber edge on average.

To quantify the deviation of L-phase flow from the assumption, an average angle of L-phase flow, θ_{ave}, is measured for each cross section perpendicular to the chamber edge at z as follows:

$$\theta_{ave}(z) = \arctan[\Sigma(\text{L−phase flow in the vertical direction})/\Sigma(\text{L−phase flow in the horizontal direction})] \quad (13)$$

where the summations are performed along the cross-section perpendicular to the chamber edge at each elevation. Elevation z is evaluated at the chamber edge for each cross-section. Then, the following parameter β_θ is reported at each elevation:

$$\beta_\theta(z) = \sin\theta_{ave}(z)/\sin\theta, \quad (14)$$

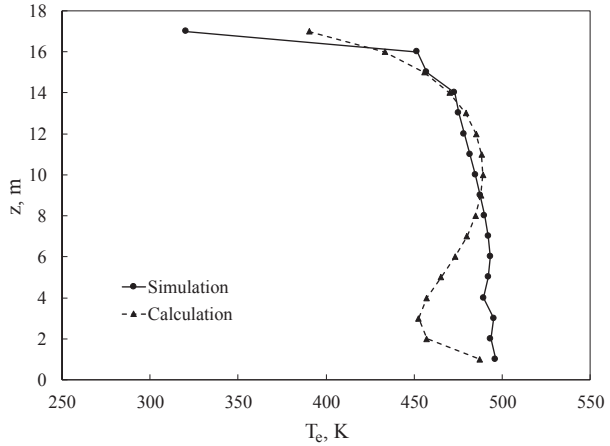

Fig. 6. Comparison of simulation and calculation results regarding chamber-edge temperature (T_e). The analytical T_e profile is close to the simulated values in the elevation range of 7–16 m at Status I.

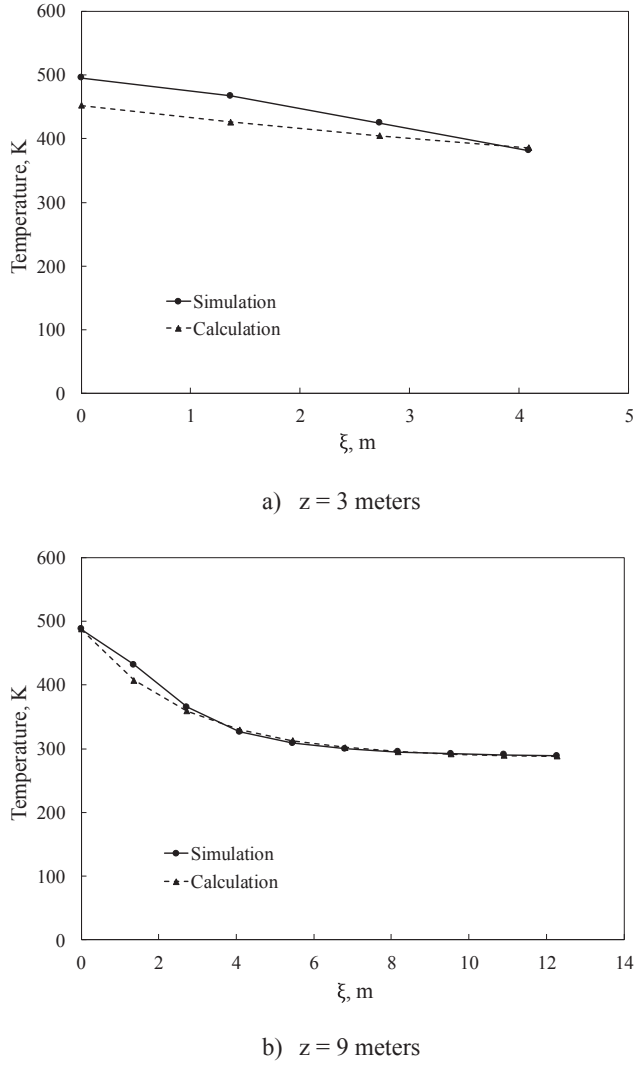

Fig. 7. Temperature distribution ahead of the chamber edge at elevations; a. 3 m, and b. 9 m. At z of 9 m near the midpoint of the chamber edge, the analytical and simulated profiles of temperature are close to each other.

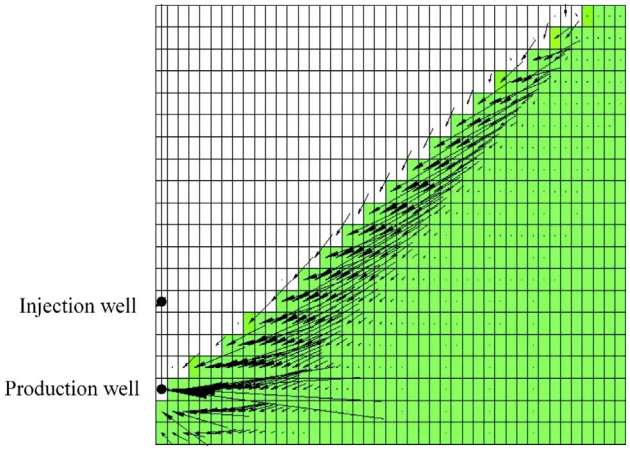

Fig. 8. Distribution of L-phase flow vectors in the simulation at Status I. Arrows in the figure represent L-phase flow directions and their magnitudes. Vapor phase saturations in white grid blocks are greater than zero; that is, white grid blocks are inside a steam chamber. Vapor phase saturations in green grid blocks are zero; that is, green grid blocks are ahead of a steam chamber. (For interpretation of the references to colour in this figure legend, the reader is referred to the web version of this article.)

Table 6
Calculation results for β_θ and k_{rave} on the basis of flow simulation results under Status I. β_θ is defined in Eq. (14), and k_{rave} is defined in Eq. (16).

	β_θ		k_{rave}	
z, m	Status I	Status II	Status I	Status II
17	−0.13	−0.22	0.91	0.99
16	0.98	1.77	0.98	0.86
15	0.52	0.82	0.97	0.89
14	1.01	0.75	0.88	0.89
13	0.88	0.73	0.91	0.88
12	0.81	0.74	0.92	0.88
11	0.80	0.79	0.91	0.87
10	0.80	0.83	0.91	0.86
9	0.81	0.68	0.91	0.89
8	0.79	0.69	0.90	0.88
7	0.74	0.71	0.90	0.87
6	0.68	0.72	0.90	0.87
5	0.64	0.71	0.90	0.86
4	0.62	0.65	0.91	0.88
3	0.71	0.64	0.88	0.87
2	0.55	0.56	0.89	0.89
1	0.38	0.41	0.89	0.91

where z is the elevation measured at the edge of a steam chamber.

Table 6 shows the β_θ values calculated based on the L-phase distribution shown in Fig. 8. Results show that the L-phase flow is closer to being parallel to the edge of a steam chamber around the midpoint elevation than near the bottom of the reservoir. Comparison between Statuses I and II in terms of β_θ indicates that the accumulation of water condensate may have affected the L-phase flow direction in the middle elevation range, but the difference in β_θ is not entirely clear in this case. The deviation of β_θ from one near the reservoir bottom can be confirmed in Fig. 8, in which L-phase flow must converge to the producing well. That is, multi-dimensional L-phase flow inevitably occurs near the reservoir bottom because of the point sink for L-phase flow, and certainly influences the heat transport there. This is likely another reason for the inaccuracy of the assumption of 1-D quasi-steady-state heat conduction from a moving boundary near the reservoir bottom.

3.2.3. *Two-phase flow ahead of a steam chamber*

As in many previous SAGD models, the developed model assumes the L-phase relative permeability to be one ahead of a steam chamber. To evaluate the two-phase flow effect on oil flow, Bharatha et al. [9] used the following equation:

$$k_{rave} = \int_{T_L}^{T_e} \frac{k_{ro}}{\nu_o(T-T_R)}dT \Big/ \int_{T_L}^{T_e} \frac{1}{\nu_o(T-T_R)}dT, \quad (15)$$

where k_{ro} is local L-phase relative permeability, and k_{rave} is average L-phase relative permeability in the cross section perpendicular to the edge of a steam chamber.

Bharatha et al. [9] did not consider variable temperature along the edge of a steam chamber; i.e., their equation does not contain elevation z. Based on Bharatha et al., this section uses the following equation to calculate average L-phase relative permeability for each cross-section perpendicular to the chamber edge:

$$k_{rave}(z) = \int_{T_{L(z)}}^{T_{e(z}} \frac{k_{ro}}{\nu_o(T-T_R)}dT \Big/ \int_{T_{L(z)}}^{T_{e(z}} \frac{1}{\nu_o(T-T_R)}dT, \quad (16)$$

where z is the elevation measured at chamber edge. k_{rave} is a function of elevation z in this equation because T_e changes along the edge of a steam chamber. Calculation with this equation uses simulated results for temperature distribution, L-phase relative permeability, and L-phase kinematic viscosity in the ξ direction (perpendicular to the steam-chamber edge) ahead of a steam chamber. The use of local temperature simulated in each grid block avoids the deviation brought by the assumed temperature profile ahead of a steam chamber in the analytical model.

Table 6 shows the calculation results at Statuses I and II. As expected, k_{rave} is calculated to be smaller than one because of the two-phase flow of oil and water ahead of a steam chamber. Comparison between the two statuses indicates that k_{rave} decreases as operation proceeds. This is because the accumulation of water condensation along the edge of a steam chamber decreases L-phase relative permeability in the mobile fluid zone (Fig. 2). This water condensate makes the drainage zone thicker ahead of a steam chamber, which causes the flow direction to deviate from being parallel to the chamber edge, especially near the production well (Fig. 2). In Table 6, the k_{rave} values do not show clear variability with respect to elevation z. Therefore, although two-phase flow systematically decreases the L-phase mobility along the edge a steam chamber, it may not directly affect temperature variation along and ahead the edge of a steam chamber. It indirectly affects the temperature variation through the effect of water accumulation on multi-dimensional flow of oil.

4. Application of the new model to the Surmont SAGD project

The developed model is based on the widely-used set of simplifying assumptions for analytical solution of SAGD. Application of such analytical models with SAGD field data is not expected to give accurate estimations of bitumen-production rate and SOR because of various complexities in actual fields, such as reservoir heterogeneity and steam-propagation conformance along the horizontal section of a SAGD well pair. However, this section presents application of the new model to the Surmont SAGD project to show the improved estimation for bitumen-production rate and SOR in comparison with other analytical models. The surmount project was selected because of the availability of field data, including chamber-edge temperature (T_e) data from an observation well.

In this section, a steam chamber is two-sided as shown in Fig. 9. Therefore, the analytical equation for bitumen-production rate, q_{prod}, is

$$q_{oil\text{-}prod} = 2\sqrt{\tau k g H \varphi \Delta S_O \Delta y^2/[2z_D(1-z_D^2)]}, \quad (17)$$

where $\tau(z) = \int_{T_L(z)}^{T_{e(z)}} \alpha/[\nu_o(T-T_R)]dT$, and $z_D = z/H$. This equation requires T_e at a given z, which should be from the middle elevation range for accurate estimation of bitumen production as discussed in the previous section. Observation-well and thermocouple data for well pair A of the Surmont SAGD project [16] give T_e of 398.27 K at z_D of 0.72, for which z_D is calculated based on the assumed chamber geometry (Fig. 9) and the lateral distance between the well pair and the observation well. Table 7 presents pertinent data for analytical calculation for well pair A of the Surmont SAGD project.

Table 8 summarizes the results obtained from the new model and other selected models, in comparison with field data. All analytical models give substantial overestimations for bitumen-production rate, but the new model yields a much improved estimation. This is mainly because the new model properly uses the actual information regarding chamber-edge temperature. All other analytical models use the steam temperature, 498.15 K, which is 100 K higher than the T_e value used for z_D of 0.72 in the new analytical model.

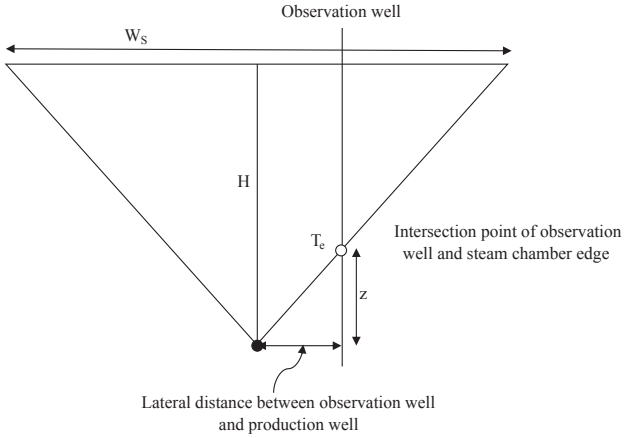

Fig. 9. Schematic for a two-sided steam chamber used for Section 4. This explains how to estimate a steam chamber-edge temperature T_e at elevation z from an observation well.

Table 7
Field data for Well Pair A for the Surmont SAGD project [16]

	Unit	ConocoPhillips Surmont Well Pair A
Initial reservoir temperature (T_R)	K	288.15
Temperature of injected steam (T_S)	K	498.15
Bitumen density (ρ_o)	kg/m^3	880
Reservoir thickness (H)	m	30
Well length (Δy)	m	850
Reservoir porosity (φ)	–	0.33
Reservoir thermal diffusivity (α)	m^2/s	7.00×10^{-7}
Permeability to oil (k)	m^2	1.00×10^{-12}
Reducible oil saturation (ΔS_o)	–	0.67
Bitumen kinematic viscosity at injection temperature (v_s)	m^2/s	3.41×10^{-6}
Temperature-viscosity parameter (m)	–	4
Heat capacity of reservoir (M_R) [27]	J/(m^3·K)	2.60×10^6
Heat capacity of overburden (M_{over}) [27]	J/(m^3·K)	2.60×10^6
Steam Quality	–	98%
Latent heat of injected steam (L_S)	J/kg	1.84×10^6
SOR	–	4
Cumulative SOR	–	3.5

Table 8
Comparison of analytical results and field data for Well Pair A of the Surmont SAGD project.

Input chamber edge temperature at the intersection (T_e, K)	398.27
Dimensionless elevation of the intersection (z_D)	0.7183
Production rate from Butler et al. [5] (m^3/day)	379
Production rate from Tandrain [6] (m^3/day)	329
Production rate from Lindrain [7] (m^3/day)	306
Production rate from Reis [8] (m^3/day)	300
Production rate from this research (m^3/day)	87
Production rate from field data (m^3/day)	36
Calculated SOR	3.0

One reason for the overestimation of bitumen-production rate is that the analytical models do not consider reservoir heterogeneity. The field operation report [16] indicates that there are mud and shale bodies that make permeability barriers in the reservoir. They affect development of a steam chamber and, therefore, heat transfer in SAGD [30]. Another reason for the overestimated bitumen-production rate is that the model assumes a steam chamber to develop along the entire horizontal section of a SAGD well pair.

The SOR estimated by the new model is 3.0, which is lower than the field value, 4.0. This is affected by the overestimated bitumen-production rate, but there are other possible reasons for the overestimated SOR. For example, the SOR calculated is sensitive to the heat capacity used and, to a lesser extent, the temperature at the reservoir top within a steam chamber. The heat capacity used (Table 7) is based on an average value for the reservoir, instead of the overlaying formation, in the absence of relevant data. The temperature at the reservoir top used in the current calculation is the steam temperature (T_S); however, actual temperatures near the reservoir top may be lower because of the effect of heterogeneity on steam-chamber growth.

5. Conclusions

This paper presented the first analytical model for SAGD with consideration of temperature variation along the edge of a steam

chamber. Since temperature is the most influential factor in SAGD, the research was originally motivated by the question as to how temperature is supposed to vary along the edge of a steam chamber for a given bitumen production rate. Analytical equations were presented for bitumen-production rate and SOR for a representative temperature at the midpoint of the edge of a steam chamber. Comparison of the analytical equations with reservoir simulations showed that they are in good agreement when the assumptions made in the analytical model are reasonably close to the simulation conditions. Conclusions are as follows:

1. Analytical solution of SAGD does not require the conventional assumption that the injected-steam temperature uniformly distributes along the edge of a steam chamber. The new model properly solves for temperature and oil-production profiles along the edge of a steam chamber by keeping the consistency between a linear chamber edge and a given oil-production rate. The constant temperature along the edge of a steam chamber (i.e., the conventional assumption) gives a concave interface of a steam chamber that is detached from the production well, like the one by Butler et al. [5]. For a chamber to exhibit a linear interface, temperature must vary along the chamber edge, which occurs in reality mainly because of heat losses to the over- and under-burden formations.
2. Prior models tend to overestimate oil-production rate substantially, because they use the injected-steam temperature as the chamber-edge temperature. Results indicate that temperature at the midpoint of the edge of a steam chamber can be used for accurate estimation of oil-production and SOR for a linear chamber edge. The chamber-edge temperature used for the new analytical model that gives accurate results can be substantially lower than the injected steam temperature for a given operating pressure in the cases tested.
3. Temperature profile ahead of a steam chamber based on steady-state 1-D heat conduction from a moving boundary is widely used in analytical models of SAGD. However, this assumption is inaccurate near the top and bottom of a reservoir. For the top section, there is 2-D heat conduction because of the heat loss to the overburden, in addition to the reservoir ahead of the chamber edge. For the bottom section, multi-dimensional heat convection due to high-temperature fluid flow is ignored in the assumed profile of temperature. Results show that the temperature profile based on steady-state 1-D heat conduction from a moving boundary is closer to the temperature profile simulated for the middle of the reservoir than to those near the top and bottom of the reservoir.
4. Application of analytical models to SAGD field data showed that the presented model gives least overestimated results in terms of bitumen-production rate in comparison with prior models [5–8]. This is mainly because the new model properly uses the actual information regarding chamber-edge temperature. All other analytical models use the steam temperature, 498.15 K, which is 100 K higher than the T_e value used for z_D of 0.72 in the new analytical model for the field case tested.

Acknowledgments

This research was funded by Japan Petroleum Exploration Co., Ltd., Japan Canada Oil Sands Ltd., and the Natural Sciences and Engineering Research Council of Canada (RGPIN 418266). Ryosuke Okuno holds the Pioneer Corporation Faculty Fellowship in Petroleum Engineering at the University of Texas at Austin.

Appendix A. Analytical equations for SAGD

The entire derivation of bitumen-production rate for SAGD's side-way expansion stage consists of the following:

Local material balance applied to a cross section perpendicular to the edge of a steam chamber
Darcy's law applied to the oil phase flowing along the chamber edge
Global material balance applied to the entire reservoir.

In Appendix A1, the first two items are combined to derive the derivative of oil flow rate with respect to elevation. In Appendix A2, previous SAGD models are discussed in terms of their assumptions and their consequences.

A1. Local material balance and Darcy's law

The assumptions made and the corresponding schematic are given in Section 2. Firstly, local material balance is applied to a cross-section perpendicular to the edge of a steam chamber, along which 1-D flow of incompressible oil occurs:

$$\frac{d}{dt}\int_0^{\infty}\int_0^{\Delta y}\varphi S_o dy d\xi + \int_0^{\infty}\int_0^{\Delta y}\frac{d}{dl}U_o dy d\xi = 0, \tag{A.1}$$

where Δy is the unit length along the horizontal section of a SAGD well pair, the ξ direction is perpendicular to the linear steam chamber edge, and U_o is the Darcy flow velocity for oil phase in the l direction (Fig. 1). Note that $\xi = 0$ at the edge of a steam chamber. The angle of the edge of a steam chamber is measured from the horizontal line as θ (Fig. 1). This angle decreases as bitumen production proceeds. Integration of Eq. (A.1) and transformation of the coordinate from l to z by dividing Eq. (A.1) by $\sin\theta$ give

$$-\varphi\Delta S_o v\Delta y + \partial q_o/\partial z = 0, \tag{A.2}$$

where v is the interface advancing velocity in the horizontal direction, and z is the elevation from the production well.

Secondly, Darcy's law is applied to the oil and vapor phases along the edge of a steam chamber. Under the assumptions made previously, oil-phase flow rate along the edge of a steam chamber is

$$U_o(z) = -k\rho_o g\sin\theta/\mu_o = -kg\sin\theta/\nu_o, \tag{A.3}$$

where k is absolute permeability, and ν_o is kinematic viscosity of oil. Integrating U_o for a cross-section perpendicular to the edge of a steam chamber, oil-flow rate at elevation z is

$$q_o(z) = \int_o^{\xi_L} U_o \Delta y d\xi = -\int_0^{\xi_L}(kg\sin\theta/\nu_o)\Delta y d\xi = -kg\sin\theta\Delta y I_o, \tag{A.4}$$

where "I_o" is defined as

$$I_o(z) = \int_0^{\xi_L} \frac{1}{\nu_o} d\xi. \tag{A.5}$$

In Eqs. (A.4) and (A.5), ξ_L is the distance from the steam-chamber edge measured along the perpendicular line until it reaches z = 0 (i.e., the production well's elevation. See Fig. 1). Note that, unlike in prior models, the integration for I_o is not from zero to infinity.

As done in previous SAGD models, 1-D steady-state heat conduction through a moving boundary [19] is used for transformation from ξ to temperature. That is, temperature distribution, T(ξ), along the cross-section originated at elevation z is

$$T(\xi,z) = T_R + [T_e - T_R]\exp[-\xi v\sin\theta/\alpha], \tag{A.6}$$

where T_e is the local chamber-edge temperature at z, vsinθ (or U in Fig. 1) is local chamber-edge advancing velocity measured at z in the normal direction, and α is thermal diffusivity of the reservoir. Temperature at ξ_L (T_L) is obtained by substituting $\xi_L = z/\cos\theta$ into Eq. (A.6); that is,

$$T_L(z) = T_R + [T_e - T_R]\exp[-vz\tan\theta/\alpha]. \tag{A.7}$$

Use of Eq. (A.6) with Eq. (A.5) enables to express I_o in terms of temperature (instead of ξ), and gives the following dimensionless variable:

$$\tau(z) = UI_o = \int_{T_L}^{T_e} \alpha/[\nu_o(T - T_R)]dT. \tag{A.8}$$

With Eq. (A.8), Eq. (A.4) is simplified as

$$vq_o + kg\tau\Delta y = 0 \tag{A.9}$$

for the cross-section perpendicular to the edge of a steam chamber at elevation z.

Combining Eqs. (A.2) and (A.9) (i.e., local material balance and Darcy's law) yields

$$\frac{\partial q_o^2}{\partial z} = -2\varphi\Delta S_o kg\tau(\Delta y)^2 \tag{A.10}$$

for the cross-section perpendicular to the edge of a steam chamber at elevation z. Appendix A2 shows that Eq. (A.10) can be used also for Butler et al.'s model and its variants.

A2. Comments on previous SAGD models

The previous SAGD models based on Butler et al. [5] and Reis [8] can be derived from the unified framework presented in this paper. This appendix presents reproduction of Butler et al.'s and Reis' equations.

For Butler et al. [5], Eq. (A.10) is integrated with the assumption that τ is constant with elevation z. That is,

$$q_o^2 = -2\varphi\Delta S_o kg\tau z(\Delta y)^2 + C, \tag{A.11}$$

where C is the constant of integration. Then, Butler's oil production rate is obtained as follows:

$$\sqrt{q_o^2|_{z=0} - q_o^2|_{z=H}} = \sqrt{2\varphi\Delta S_o kg\tau_B H}\,(\Delta y), \tag{A.12}$$

where $\tau_B = \alpha/m\nu_s$ and $\nu_s = \nu_o[(T - T_R)/(T_e - T_R)]^m$. The negative solution was discarded. From Eq. (A.11), oil-flow rate of Butler et al. [5] can be given as a function of elevation as follows:

$$q_o = -\sqrt{2\varphi\Delta S_o kg\tau_B H(1 - z_D)}\,(\Delta y). \tag{A.13}$$

Use of Eqs. (A.9) and (A.13) gives the chamber-advancing velocity, v, as a function of elevation z, which indicates the well-known concave interface of Butler's steam chamber.

For Reis' model, Eq. (A.9) has to be replaced by

$$v_{max}q_o|_{z=0} + kg\tau_R\Delta y = 0, \tag{A.14}$$

where $\tau_R = \tau_B/a$ and a was assumed to be 0.4 by Reis [8]. Then, Eq. (A.14) is applied to the global material balance for an inverted triangle, which results in

$$q_o|_{z=0} = -\sqrt{0.5\varphi\Delta S_o kg\tau_R H}\,(\Delta y). \tag{A.15}$$

Eq. (A.14) is somewhat inconsistent because v_{max} is v at the reservoir top (z = H), but q_o is evaluated at the production well (z = 0). This inconsistency is obvious by comparing Eq. (A.14) with Eq. (A.9), which is Darcy's law applied locally at elevation z for the cross-section perpendicular to the edge of a steam chamber. Furthermore, the assumption of the constant $\tau_R = \tau_B/a$ is inconsistent with Reis' own assumption of a linear chamber edge; that is, as shown in this paper, variation of τ with respect to z is required for a chamber edge to be linear.

Appendix B. Steam-Oil ratio calculation

The heat injected mainly goes to four parts: heat carried by produced oil (Q_{PO}), heat loss to the overburden formation rocks (Q_{OB}), heat inside a steam chamber (Q_{SC}), and heat ahead of a steam chamber (Q_{AC}). The derivation of SOR shown here is based on a half of a steam chamber, which is the same as the derivation of production rate in Section 2. Because a steam chamber is assumed to be an inverted triangle, it has a large contact area with the overburden rocks at a high temperature of the steam chamber. This causes a large amount of heat loss to the overburden formation. Temperature on the interface between the reservoir and underlying formation is relatively low; hence, there is a limited heat loss to the underlying formation. Heat loss to underlying formation rocks is omitted in the calculation as in previous studies [8,13,29,31].

Instantaneous SOR can be calculated by the following energy balance equation:

$$Q'_{inj} = Q'_{SC} + Q'_{AC} + Q'_{OB} + Q'_{PO}, \tag{B.1}$$

where Q'_{inj} is the injection rate of latent heat carried by the injected steam in J/s; Q'_{SC} is the rate of heat required for chamber expansion in J/s; Q'_{AC} is the rate of heat used for the reservoir ahead of the edge of a steam chamber in J/s; Q'_{OB} is the rate of heat loss to the overburden formation in J/s; and Q'_{PO} is the rate of heat carried by produced bitumen in J/s. The sensible heat of hot water is not considered under the assumption that the heat carried by the produced hot water is equal to the sensible heat of the injected steam.

Q'_{SC} can be calculated by the increasing rate of heat inside the steam chamber. Heat inside a half steam chamber is

$$Q_{SC} = 0.5M_R(T_S - T_R)W_S H\Delta y, \tag{B.2}$$

where W_S is the width of the top (ceiling) of the half steam chamber, M_R is the volumetric heat capacity of reservoir. Thus, the rate Q'_{SC} can be expressed as

$$Q'_{SC} = dQ_{SC}/dt = 0.5M_R(T_S - T_R)(dW_S/dt)Hdy = 0.5M_R(T_S - T_R)v_{max}H\Delta y. \tag{B.3}$$

To obtain Q'_{AC}, the heat stored in the reservoir ahead of the edge of a steam chamber is calculated.

$$d^2Q_{AC} = M_R(T - T_R)d\xi dl\Delta y, \tag{B.4}$$

where dl is the unit length in the upward direction along the edge of a steam chamber. Then, a temperature distribution ahead of a steam chamber is obtained by the one-dimensional steady state conduction. According to Carslaw and Jaeger [19], it is expressed as

$$(T - T_R)/[T_{e(z)} - T_R] = \exp[-U_{(z)}\xi/\alpha] = \exp(-\xi v_{max}z_D\sin\theta/\alpha). \tag{B.5}$$

Substitution of Eq. (B.5) into Eq. (B.4) yields

$$d^2Q_{AC(z)} = M_R[T_{e(z)} - T_R]\exp(-\xi v_{max}z_D\sin\theta/\alpha)d\xi dl\Delta y. \tag{B.6}$$

Eq. (B.6) can be integrated from $\xi = 0$ to the level of the production well in the perpendicular direction, as follows:

$$dQ_{AC(z)} = M_R[T_{e(z)} - T_{L(z)}]\alpha dl\Delta y/(v_{max}z_D\sin\theta). \tag{B.7}$$

The unit length of the steam-chamber edge, dl, can be expressed as $dl = dz/\sin\theta$. Hence, Eq. (B.7) becomes

$$dQ_{AC(z)} = M_R[T_{e(z)} - T_{L(z)}]\alpha dz\Delta y/(v_{max}z_D\sin^2\theta). \tag{B.8}$$

To obtain Q_{AC}, Eq. (B.8) is integrated in terms of elevation, z, as shown in Fig. 1. The temperature at the edge of a steam chamber (T_e) varies with z. To simplify the calculation in this research, T_e is considered constant for a layer of one-meter thickness. Thus, Q_{AC} is expressed as a summation of the heat residing ahead of a steam chamber for each one-meter layer with the corresponding T_e. Thus, integration of Eq. (B.8) yields

$$Q_{AC} = \sum_{i=1}^{N_L} M_R[T_{e(z)} - T_{L(z)}]\alpha h_i\Delta y/(v_{max}z_D\sin^2\theta), \tag{B.9}$$

where N_L is the number of one-meter layers, and h_i is set to one meter in this paper.

Then, Q'_{AC} is

$$Q'_{AC} = dQ_{AC}/dt = -\sum i{=}1^{N_L} 2M_R[T_{e(z)} - T_{L(z)}]\alpha h_i\sin^{-3}\theta\cos\theta\Delta y/(v_{max}z_D)(d\theta/dt). \tag{B.10}$$

According to the linear geometry assumed for a steam chamber, the angle between the steam chamber edge and horizontal line can be expressed as

$$\theta = \arctan(H/W_S). \tag{B.11}$$

Therefore,

$$d\theta/dt = -Hv_{max}/(H^2 + W_S^2). \tag{B.12}$$

Substitution of Eq. (B.12) into Eq. (B.10) gives

$$Q'_{AC} = \sum i{=}1^{N_L} 2M_R[T_{e(z)} - T_{L(z)}]\alpha h_i\Delta y/(z\tan\theta). \tag{B.13}$$

The heat loss to the overburden (Q_{OB}) is given by

$$Q_{OB} = -\alpha M_{over}\int_0^{W_S}\frac{dT}{dz}|_{z=H}(t-\sigma)dW\Delta y, \tag{B.14}$$

where M_{over} is volumetric heat capacity of the overburden formation, σ is the time since the steam zone reached a specific width, t is the time since the commencement of operation, α is the thermal diffusivity of the reservoir, and $\frac{dT}{dz}|_{z=H}$ can be obtained according to the one-dimensional unsteady-state heat transfer equation of Carslaw and Jaeger [19]. The temperature at the bottom of the overburden formation ($T_{ceiling}$) is equal to the overburden formation. It is temperature at the contact area between the steam chamber and assumed that $T_{ceiling}$ is constant all over the contact area in the deviation. Then,

$$Q_{OB} = 2M_{over}(T_{ceiling} - T_R)\sqrt{\alpha/\pi}\int_0^{W_S}\sqrt{(t-\sigma)}dW\Delta y = (4/3)M_{over}(T_{ceiling} - T_R)\sqrt{\alpha/(\pi v_{max})}W_S^{\frac{3}{2}}\Delta y. \tag{B.15}$$

The heat-loss rate to overburden (Q'_{OB}) is

$$Q'_{OB} = dQ_{OB}/dt = 2M_{over}(T_{ceiling} - T_R)\Delta y\sqrt{\alpha v_{max}W_S/\pi}. \tag{B.16}$$

When it is reasonable to assume $T_{ceiling}$ to be the steam-chamber temperature (T_S), Eq. (B.16) becomes

$$Q'_{OB} = 2M_{over}(T_S - T_R)\Delta y\sqrt{\alpha v_{max} W_S/\pi}. \quad (B.17)$$

The amount of heat carried by the produced oil is:

$$Q'_{PO} = q_o(T_S - T_R)M_o, \quad (B.18)$$

where q_o is the oil production rate and can be obtained by the analytical model presented in this paper. M_o is the volumetric heat capacity of the produced oil. The temperature of the produced oil is assumed to be T_S.

The relationship between the rate of the injected steam (CWE, cold water equivalent in m^3/s), q_s, and the rate of the heat provided can be expressed as

$$q_s = Q'_{inj}/(\rho_w L_s x), \quad (B.19)$$

where ρ_w is the volumetric density of water in kg/m^3, L_S is the latent heat carried by the injected steam in J/kg and x is steam quality.

In summary, steam injection rate can be calculated by combining the above equations as

$$q_s = [1/(\rho_w L_s x)]\{0.5M_R(T_S - T_R)v_{max}H\Delta y + \sum 2M_R[T_{e(z)} - T_{L(z)}]\alpha h\Delta y/(z\tan\theta) + 2M_{over}(T_{ceiling} - T_R)\Delta y\sqrt{\alpha v_{max} W_S/\pi} + q_{prod}(T_S - T_R)M_o\}. \quad (B.20)$$

$$SOR = q_s/q_{oil-prod}. \quad (B.21)$$

References

[1] Mehrotra AK, Svrcek WY. Viscosity of compressed athabasca bitumen. Can J Chem Eng 1986;64(5):844–7.
[2] Nasr TN, Beaulieu G, Golbeck H, Heck G. Novel expanding solvent-SAGD process "ES-SAGD". J Can Pet Technol 2003;42(1):13–6.
[3] Gupta S, Gittins S, Picherack P. Field implementation of solvent aided process. J Can Pet Technol 2005;44(11):8–13.
[4] Keshavarz M, Okuno R, Babadagli T. Optimal application conditions for steam/solvent coinjection. SPE Reservoir Eval Eng 2015;18(1):20–38.
[5] Butler RM, McNab GS, Lo HY. Theoretical studies on the gravity drainage of heavy oil during in-situ steam heating. Can J Chem Eng 1981;59:455–60.
[6] Butler RM, Stephens DJ. The Gravity drainage of steam-heated heavy oil to parallel horizontal wells. J Can Pet Technol 1981;20(2):90–6.
[7] Butler RM. Horizontal Wells for the Recovery of Oil, Gas and Bitumen, Petroleum Society Monograph Number 2. Canadian Institute of Mining, Metallurgy & Petroleum; 1994.
[8] Reis JC. A steam-assisted gravity drainage model for tar sands: linear geometry. J Can Pet Technol 1992;31(10):14–20.
[9] Bharatha S, Yee CT, Chan MY, Dissolved Gas Effects in SAGD. Presented at the Canadian International Petroleum Conference, Calgary, Alberta, Canada, 7–9 June; 2005.
[10] Sharma J, Gates ID. Multiphase flow at the edge of a steam chamber. Can J Chem Eng 2010;88(3):312–21.
[11] Mojarad M, Dehghanpour H. Analytical modeling of emulsion flow at the edge of a steam chamber during a steam-assisted-gravity-drainage process. SPE J 2016;21(2):353–63.
[12] Cokar M, Kallos MS, Gates ID. A new thermogeomechanical theory for gravity drainage in steam-assisted gravity drainage. SPE J 2013;18(04):736–41. SPE-163136-PA.
[13] Irani M, Cokar M. Discussion on the Effect of temperature on thermal properties in the Steam-Assisted-Gravity-Drainage (SAGD) process. Part 1: thermal conductivity. SPE J 2016;21(02):334–52.
[14] Akin S. Mathematical modeling of steam-assisted gravity drainage. SPE Reservoir Eval Eng 2005;8(5):372–6.
[15] Azad A, Chalaturnyk RJ. A mathematical improvement to SAGD using geomechanical modelling. J Can Pet Technol 2010;49(10):53–64.
[16] ConocoPhillips Surmont SAGD 9426 & 9460. ERCB Annual Update: Surmont Project. 2007 & 2008.
[17] Sheng J. Enhanced oil recovery field case studies. Elsevier; 2013.
[18] Shi X. Analytical solution for SAGD with consideration of temperature variation along the edge of a steam chamber. Canada: University of Alberta; 2016. http://dx.doi.org/10.7939/R3W669M7F. [Master's thesis].
[19] Carslaw HS, Jaeger JC. Conduction of heat in solids. Second ed. Oxford Science Publications; 1959.
[20] Computer Modelling Group (CMG) Ltd. User Manual. Version 2014. Calgary, Alberta, Canada, 2014.
[21] Kumar A, Okuno R. Reliable characterization of bitumen based on perturbation from n-alkanes for steam-solvent coinjection simulation. Fuel 2016;182:141–53.
[22] Peng DY, Robinson DB. The Characterization of the Heptanes and Heavier Fractions for the GPA Peng-Robinson Programs. Gas Processors Association Research Report RR-28, 1978.
[23] Venkatramani A, Okuno R. Compositional mechanisms in steam-assisted gravity drainage and expanding-solvent steam-assisted gravity drainage with consideration of water solubility in oil. SPE Reservoir Eval Eng 2016.
[24] Venkatramani A, Okuno R. Characterization of water containing oil using an EOS for steam injection processes. J Nat Gas Sci Eng 2015;26:1091–106.
[25] Glandt CA, Chapman WG. Effect of water dissolution on oil viscosity. SPE Reservoir Eng 1995;10(1):59–64. http://dx.doi.org/10.2118/24631-PA. SPE-24631-PA.
[26] Amani MJ, Gray MR, Shaw JM. Phase behavior of athabasca bitumen water mixtures at high temperature and pressure. J Supercritical Fluids 2013;77:142–52. http://dx.doi.org/10.1016/j.supflu.2013.03.007.
[27] Amani MJ, Gray MR, Shaw JM. Volume of mixing and solubility of water in athabasca bitumen at high temperature and pressure. Fluid Phase Equilib 2013;358:203–11. http://dx.doi.org/10.1016/j.fluid.2013.07.021.
[28] Butler RM. A new approach to modelling steam assisted gravity drainage. J Can Pet Technol 1985;24(3):42–51.
[29] Keshavarz M, Harding T, Chen Z. Modification of Butler's Unsteady-State SAGD Theory to Include the Vertical Growth of Steam Chamber. Presented at the SPE Heavy Oil Technical Conference, Calgary, Alberta, Canada, 7–9, June; 2016.
[30] Venkatramani A, Okuno R. Steam-Solvent Coinjection under Reservoir Heterogeneity: Should ES-SAGD be Implemented for Highly Heterogeneous Reservoirs? Presented at the SPE Heavy Oil Technical Conference, Calgary, Alberta, Canada, 14–16 February; 2017.
[31] Zargar Z, Farouq Ali SM, Analytical Treatment of SAGD - Old and New. Presented at the SPE Canada Heavy Oil Technical Conference, Calgary, Alberta, Canada, 7–9, June 2016.